Scilight

Complex Systems Stability & Control
https://www.sciltp.com/journals/cssc

Article

Adaptive Synchronization of a Category of Neural Networks with Proportional Delays

Qian Yan [1], Xiao Han [1], Liqun Zhou [1,2,*] and Mengran Zheng [1,2]

[1] School of Mathematics Science, Tianjin Normal University, Tianjin 300387, China
[2] Institute of Mathematics and Interdisciplinary Sciences, Tianjin Normal University, Tianjin 300387, China
* Correspondence: liqunzhou@tjnu.edu.cn

How To Cite: Yan, Q.; Han, X.; Zhou, L; et al. Adaptive Synchronization of a Category of Neural Networks with Proportional Delays. *Complex Systems Stability & Control* **2025**, *1*(1), 6.

Received: 30 September 2025
Revised: 8 November 2025
Accepted: 17 November 2025
Published: 24 November 2025

Abstract: This article delves into the adaptive synchronization of a category of proportional delay neural networks (PDNNs) in the drive-response framework, with a focus on exploring their global polynomial synchronization (GPS) and global asymptotic synchronization (GAS). By introducing polynomial functions, designing adaptive controllers, and constructing appropriate Lyapunov functional, the criteria for achieving adaptive synchronization in the studied system are obtained. Furthermore, the validity of the derived criteria is confirmed by means of a numerical example and simulations. Finally, the GPS control result of the numerical example is applied to the field of image encryption, and the effectiveness of adaptive control is verified through the application of image encryption.

Keywords: proportional delay; neural networks; adaptive control; global polynomial synchronization; global asymptotic synchronization; encryption and decryption of image

1. Introduction

Neural networks (NNs) are computational models that process information by simulating the connection, patterns between neurons in the human brain. Since Hopfield proposed the landmark Hopfield NNs [1] in 1984, NNs have experienced leapfrog development. At present, the research on theory and applications of NNs has become a hot topic in international frontier research. In the past few decades, NNs have not only established a complete disciplinary system, but also demonstrated outstanding application value in multiple interdisciplinary fields such as image processing, intelligent control systems, pattern recognition and artificial intelligence, data clustering analysis, signal processing, and medical health diagnosis.

In the actual operation process of NNs, limited by the inherent switching speed of amplifiers during signal transmission, the delayed phenomenon becomes an inevitable characteristic. This phenomenon not only stems from the physical limitations of the hardware itself, but also results from the fact that NNs need to meet specific dynamic properties in various applications. Therefore, in-depth research on the dynamic behavior of delayed NNs (DNNs) can not only deepen theoretical understanding, but also provide important support for practical applications. Since Pecora and Carroll introduced the concept of master-slave system synchronization in [2] in 1990, a great deal of research has been carried out on the synchronization of diverse systems. Over the past few years, there have been relatively abundant studies achievements on the synchronization problem of bounded time-varying DNNs. For example, in [3], relying on the Lyapunov stability method, by designing an adaptive controller, the GAS criteria for uncertain dynamic networks with coupling delays were derived. In [4], the theory of discontinuous right-hand-side differential equations proposed by Filippov and the design of an adaptive controller were adopted to analyze the adaptive synchronization of memristive DNNs. Adaptive control is an advanced control method that can automatically adjust the controller parameters to adapt to the changes in the dynamic characteristics of the controlled object.

Proportional delay, as an unbounded time-varying delay, exerts a crucial influence on areas like QoS (Quality of Service) routing decision-making. In 2011, based on the need for proportional delay guarantee in QoS routing

decision-making [5] and the theoretical basis that it can be implemented by NNs, Zhou innovatively proposed the PDNNs [6]. Since then, the dynamic characteristics of PDNNs have been deeply studied, such as stability [7–10], stabilization [11–16], passivity [17–20], dissipativity [21–25], periodicity [26–30], etc. The synchronization of PDNNs has also received extensive attention [31–42]. Constructing Lyapunov functionals is the core method that is most widely used and has the highest recognition in current research on the synchronization of PDNNs. Combining this method with a differentiated controller design can flexibly achieve the synchronous control of different types of PDNNs. As in [31–33], the GPS and fixed-time synchronization of several types of PDNNs have been achieved by designing feedback controllers. In [34–36], though designing adaptive controllers, the GPS and exponential lag synchronization of several PDNNs are discussed, respectively. More specifically, in [37,38], feedback controllers and adaptive controllers were designed for two types of memristive PDNNs (MPDNNs), respectively, achieving finite-time synchronization and GAS. In [39], the advantages of adaptive control and sliding mode control are innovatively integrated to devise an adaptive sliding mode controller, which realizes the GPS of MPDNNs with uncertainty. In [40,41], by designing a switching controller, the fixed-time synchronization and general decay synchronization of two types of memristive competitive PDNNs were realized. In addition to the above mainstream approaches based on Lyapunov functionals, the academic community is also exploring other synchronization analysis methods for PDNNs. As in [42], a feedback controller is adopted to establish a new proportional delay differential inequality, which can further realize the GPS of memristive competitive PDNNs with uncertain parameters. However, due to the unboundedness of the proportional delay, the research on the synchronization of PDNNs is still relatively scarce.

Based on the above discussion, this paper focuses on a type of PDNNs. By introducing polynomial functions, designing an adaptive controller, and constructing appropriate Lyapunov functional, it explores the adaptive synchronization of the PDNNs, including GPS and GAS. The innovation and main contributions of this paper are summarized below:

(1) In contrast to earlier studies [3, 43] whose methods were only applicable to constant delay systems and struggled to accurately characterize time-varying delay properties, and although [44] introduced a time-varying delay model that relaxes fixed constraints, it still requires bounded derivative conditions to ensure stability, which fundamentally restricts the dynamic variations of the delay. Compared to these results, the proportional delay system studied in this paper features unbounded time-varying delays, and its analysis does not require restricting the rate of change of the delay.

(2) Current dynamical analysis methods for PDNNs typically employ nonlinear transformation technique [6,11], which convert PDNNs into constant DNNs through nonlinear transformation, and then apply the dynamic methods of constant DNNs for analysis. The limitations of this approach lie in the complexity of the conversion process and the highly conservative nature of the obtained results. This paper abandons traditional dynamical analysis methods for PDNNs and directly investigates NNs synchronization under proportional delay conditions. The proposed methodology demonstrates universality and can be extended to analyze dynamic characteristics of other PDNNs.

(3) Reference [45] investigated the GAS of Cohen-Grossberg PDNNs through the design of an adaptive controller. By contrast, this paper introduces polynomial functions to design adaptive controllers and Lyapunov functional for studying GPS of PDNNs. The convergence rate of GPS is higher than that of conventional GAS. Therefore, the findings of this paper further develop the research achievements of [45]. In the derivation of Theorem 1, we utilized the definition and properties of the 2-norm to construct a Lyapunov functional and scaling inequalities, which were rarely seen in previous studies.

(4) Compared with the controller in [31–33,39–41], our adaptive controller has key advantages: it enables online learning for auto-adapting to parameter changes, works without prior system knowledge, eliminates chattering, needs no fixed control mode, and thus performs better in robustness and accuracy, for time-varying delay systems—e.g. the proportional delay system here. For detailed comparison, as shown in Table 1.

Table 1. Simplified comparison of control strategies.

Aspect	**[39]**	**[40,41]**	**[31–33]**	**This Paper**
Control	Sliding Mode	Switching	Feedback	Adaptive
Core Idea	Strong rejection of disturbances	Multi-controller switching	Error-based adjustment	Self-adjusting parameters
Main Drawback	Chattering	Switching instability	Poor adaptability	Complex design
Tuning	Manual	Manual multiple	Manual	Self-tuning
Model Need	Disturbance bounds	Multiple models	Accurate model	Basic structure

2. Model Description and Prerequisite Knowledge

Notations 1. *$\mathbb{R}, \mathbb{R}_+$ and $\mathbb{R}^n$ respectively represent the set of real numbers, the set of positive real numbers, and the n-dimensional Euclidean space. For $x = (x_1, x_2, \cdots, x_n)^T = col(x_i) \in \mathbb{R}^n$, $\|x\| = \sqrt{\sum_{i=1}^{n} x_i^2}$. $C([\overline{q}t_0, t_0], \mathbb{R}^n) \triangleq C$ indicates the set consisting of all continuous functions from $[\overline{q}t_0, t_0]$ to $\mathbb{R}^n$. $\{1, 2, \cdots, n\} \triangleq \hat{n}$. E represents the identity matrix of the corresponding dimension. For matrix $A > 0$, it indicates that A is positive definite.*

Consider the following class of PDNNs:

$$\begin{cases} \dot{u}(t) = -Au(t) + Bf(u(t)) + Cg(u(qt)), t \geq t_0 \geq 0, \\ u(s) = \phi(s), s \in [\overline{q}t_0, t_0], \overline{q} = \min\limits_{i \in \hat{n}}\{q_i\}, \end{cases} \tag{1}$$

where

$u(t) = (u_i(t)) \in \mathbb{R}^n$	State variable
$A = \mathrm{diag}(a_1, a_2, \ldots, a_n) > 0$	Self-feedback matrix
$B = (b_{ij})_{n\times n}$ and $C = (c_{ij})_{n\times n}$	Connection weight matrices
$q_i \in (0, 1)$	Proportional delay factors
$\phi(s) = (\phi_i(s)) \in C([\overline{q}t_0, t_0], \mathbb{R}^n)$	Initial function
$(1 - q_i)t \to +\infty$ (as $t \to +\infty$)	Proportional delay transfer function
$f(\cdot)$ and $g(\cdot)$	Activation functions with

$f(u(t)) = (f_i(u_i(t))) \in \mathbb{R}^n$, $g(u(qt)) = (g_1(u_1(q_1t)), g_2(u_2(q_2t)), \cdots, g_n(u_n(q_nt)))^T$

This paper takes system (1) as the driving system and selects the corresponding response system as:

$$\begin{cases} \dot{v}(t) = -Av(t) + Bf(v(t)) + Cg(v(qt)) + \Theta(t), \ t \geq t_0 \geq 0, \\ v(s) = \varphi(s), \ s \in [\overline{q}t_0, t_0], \end{cases} \tag{2}$$

where $v(t) = (v_i(t)) \in \mathbb{R}^n$; $\varphi(s) = (\varphi_i(s)) \in C([\overline{q}t_0, t_0], \mathbb{R}^n)$; $\Theta(t) = (\theta_i(t)) \in \mathbb{R}^n$ is a controller.

Let $e(t) = v(t) - u(t)$, the error system of systems (1) and (2) becomes

$$\begin{cases} \dot{e}(t) = -Ae(t) + Bf(e(t)) + Cg(e(qt)) + \Theta(t), \ t \geq t_0 \geq 0, \\ e(s) = v(t) - u(t), \ s \in [\overline{q}t_0, t_0], \end{cases} \tag{3}$$

where $f(e(t)) = f(v(t)) - f(u(t))$, $g(e(qt)) = g(v(qt)) - g(u(qt))$.

This paper provides the following definitions and assumption.

Definition 1. *Systems (1) and (2) can achieve global asymptotic synchronization (GAS). Under the appropriate controller $\Theta(t)$, if for any initial function $\phi(s)$, $\varphi(s) \in C([\overline{q}t_0, t_0], \mathbb{R}^n)$, such that [46]*

$$\lim_{t\to+\infty} \|v(t) - u(t)\| = 0, t \geq t_0 \geq 0.$$

Definition 2. *Systems (1) and (2) can achieve global polynomial synchronization (GPS). Under the appropriate controller $\Theta(t)$, if for any initial function $\phi(s)$, $\varphi(s) \in C([\overline{q}t_0, t_0], \mathbb{R}^n)$, there exist constants $M \geq 1$ and $\theta \geq 0$, such that [31]*

$$\|v(t) - u(t)\|^2 \leq M \sup_{\overline{q}t_0 \leq s \leq t_0} \|\varphi(s) - \phi(s)\|^2 (1 + t)^{-\theta}, t \geq t_0 \geq 0.$$

Assumption 1. *For any $\xi, \eta \in \mathbb{R}, j \in \hat{n}$, there exist constants $h_j > 0$ and $l_j > 0$, such that*

$$|f_j(\xi) - f_j(\eta)| \leq h_j|\xi - \eta|; |g_j(\xi) - g_j(\eta)| \leq l_j|\xi - \eta|.$$

3. Main Results

In this article, we introduce a polynomial function $(1 + t)^\theta$ to design the following adaptive controller:

$$\Theta(t) = -k(t)e(t), \tag{4}$$

where $k(t)$ represents the gain coefficient function, $\dot{k}(t) = \varepsilon(1 + t)^\theta e(t)^T e(t), k(0) \geq 0, \varepsilon > 0, \theta > 0$.

Theorem 1. *If Assumption 1 holds, then systems (1) and (2) can achieve GPS under controller (4).*

Proof. Constructing Lyapunov functional given below

$$V(t) = V_1(t) + V_2(t),$$

with

$$V_1(t) = \frac{1}{2}(1+t)^{\theta} e(t)^T e(t) + \frac{1}{2\varepsilon}(k(t)-k^*)^2,$$

$$V_2(t) = \frac{1}{2} l \|C\| \sum_{j=1}^{n} q_j^{-1} \int_{q_j t}^{t} (1+q_j^{-1}s)^{\theta} e_j^2(s) \mathrm{d}s,$$

where $k^* \in \mathbb{R}$, $l = \max_{i\in\hat{n}}\{l_i\}$.

Differentiating $V_1(t)$ with respect to system (3), and substituting controller (4) into it, we have

$$\begin{aligned}
\dot{V}_1(t) &= (1+t)^{\theta} e(t)^T \dot{e}(t) + \frac{1}{2}\theta(1+t)^{\theta-1} e(t)^T e(t) + \frac{1}{\varepsilon}(k(t)-k^*)\dot{k}(t) \\
&= (1+t)^{\theta} e(t)^T [-Ae(t) + Bf(e(t)) + Cg(e(qt)) - k(t)e(t)] \\
&\quad + \frac{1}{2}\theta(1+t)^{\theta-1} e(t)^T e(t) + (k(t)-k^*)(1+t)^{\theta} e(t)^T e(t) \\
&\leq -a_{\min}(1+t)^{\theta} e(t)^T e(t) + (1+t)^{\theta} \|B\| \|e(t)\| \|f(e(t))\| \\
&\quad + (1+t)^{\theta} \|C\| \|e(t)\| \|g(e(qt)) + [\frac{1}{2}\theta(1+t)^{\theta-1} - (1+t)^{\theta} k^*] e(t)^T e(t),
\end{aligned} \tag{5}$$

where $a_{\min} = \min_{i\in\hat{n}}\{a_i\}$.

From Assumption 1, we obtain

$$\begin{aligned}
\|f(e(t))\| &= \sqrt{f(e(t))^T f(e(t))} = \sqrt{\sum_{i=1}^{n} f_i^2(e_i(t))} \\
&\leq \sqrt{\sum_{i=1}^{n} h_i^2 e_i^2(t)} \leq h\|e(t)\|,
\end{aligned} \tag{6}$$

$$\|g(e(qt))\| \leq \sqrt{\sum_{i=1}^{n} l_i^2 e_i^2(qt)} \leq l\|e(qt)\|, \tag{7}$$

where $h = \max_{i\in\hat{n}}\{h_i\}$.

Substituting (6) and (7) into (5), we get

$$\begin{aligned}
\dot{V}_1(t) &\leq -a_{\min}(1+t)^{\theta} e(t)^T e(t) + h(1+t)^{\theta} \|B\| e(t)^T e(t) \\
&\quad + l(1+t)^{\theta} \|C\| \|e(t)\| \|e(qt)\| + \left[\frac{1}{2}\theta(1+t)^{\theta-1} - (1+t)^{\theta} k^*\right] e(t)^T e(t) \\
&\leq -a_{\min}(1+t)^{\theta} e(t)^T e(t) + h(1+t)^{\theta} \|B\| e(t)^T e(t) \\
&\quad + \frac{1}{2} l(1+t)^{\theta} \|C\| e(t)^T e(t) + \frac{1}{2} l(1+t)^{\theta} \|C\| e(qt)^T e(qt) \\
&\quad + \left[\frac{1}{2}\theta(1+t)^{\theta-1} - (1+t)^{\theta} k^*\right] e(t)^T e(t) \\
&\leq \left[-a_{\min} + h\|B\| + \frac{1}{2} l\|C\| + \frac{\theta}{2} - k^*\right] (1+t)^{\theta} e(t)^T e(t) \\
&\quad + \frac{1}{2} l\|C\| (1+t)^{\theta} e(qt)^T e(qt).
\end{aligned} \tag{8}$$

We differentiate $V_2(t)$ along system (3) and obtain

$$\begin{aligned}\dot{V}_2(t) &= \frac{1}{2}l\|C\|\sum_{j=1}^{n} q_j^{-1}\left[(1+q_j^{-1}t)^{\theta}e_j^2(t) - (1+t)^{\theta}e_j^2(q_jt)q_j\right] \\ &\leq \frac{1}{2}l\|C\|\left[\overline{q}^{-1}(1+\overline{q}^{-1}t)^{\theta}e^T(t)e(t) - (1+t)^{\theta}e^T(qt)e(qt)\right].\end{aligned} \tag{9}$$

According to (8) and (9), we have

$$\begin{aligned}\dot{V}(t) &\leq \left[-a_{\min} + h\|B\| + \frac{1}{2}l\|C\| + \frac{\theta}{2} - k^*\right](1+t)^{\theta}e(t)^Te(t) \\ &\quad + \frac{1}{2}l\|C\|(1+t)^{\theta}e(qt)^Te(qt) + \frac{1}{2}l\|C\|\left[\overline{q}^{-1}(1+\overline{q}^{-1}t)^{\theta}e^T(t)e(t)\right. \\ &\quad \left. - (1+t)^{\theta}e^T(qt)e(qt)\right] \\ &\leq \left[-a_{\min} + h\|B\| + \frac{1}{2}l\|C\| + \frac{1}{2}l\|C\|\overline{q}^{-1}(1+\overline{q}^{-1}t)^{\theta}(1+t)^{-\theta} + \frac{\theta}{2} - k^*\right] \\ &\quad \times (1+t)^{\theta}e(t)^Te(t) \\ &\leq \left[-a_{\min} + h\|B\| + \frac{1}{2}l\|C\| + \frac{1}{2}l\|C\|\overline{q}^{-1}(1+\overline{q}^{-1}t_0)^{\theta}(1+t_0)^{-\theta} + \frac{\theta}{2} - k^*\right] \\ &\quad \times (1+t)^{\theta}e(t)^Te(t).\end{aligned} \tag{10}$$

Choosing $k^* = h\|B\| + \frac{1}{2}l\|C\| + \frac{1}{2}l\|C\|\overline{q}^{-1}(1+\overline{q}^{-1}t_0)^{\theta}(1+t_0)^{-\theta} + \frac{\theta}{2}$. From (10), we get

$$\dot{V}(t) \leq -a_{\min}(1+t)^{\theta}e(t)^Te(t) \leq 0.$$

Then for any $t \geq t_0$, the above formula implies that

$$V(t) \leq V(t_0), \tag{11}$$

where

$$\begin{aligned}V(t_0) &= \frac{1}{2}(1+t_0)^{\theta}\|e(t_0)\|^2 + \frac{1}{2\varepsilon}(k(t_0)-k^*)^2 + \frac{1}{2}l\|C\|\sum_{j=1}^{n} q_j^{-1}\int_{q_jt_0}^{t_0}(1+q_j^{-1}s)^{\theta}e_j^2(s)\mathrm{d}s \\ &\leq \frac{1}{2}(1+t_0)^{\theta}\sup_{\overline{q}t_0\leq s\leq t_0}\|\varphi(s)-\phi(s)\|^2 + M_1 \\ &\quad + \frac{1}{2}l\overline{q}\|C\|\sup_{\overline{q}t_0\leq s\leq t_0}\|\varphi(s)-\phi(s)\|^2\sum_{j=1}^{n}\int_{q_jt_0}^{t_0}(1+q_j^{-1}s)^{\theta}\mathrm{d}s \\ &\leq \frac{1}{2}(1+t_0)^{\theta}\sup_{\overline{q}t_0\leq s\leq t_0}\|\varphi(s)-\phi(s)\|^2 + M_1 \\ &\quad + \frac{1}{2(\theta+1)}l\overline{q}\|C\|\sup_{\overline{q}t_0\leq s\leq t_0}\|\varphi(s)-\phi(s)\|^2\sum_{j=1}^{n}q_j\left[(1+q_j^{-1}t_0)^{\theta+1} - (1+t_0)^{\theta+1}\right] \\ &\leq \frac{1}{2}(1+t_0)^{\theta}\sup_{\overline{q}t_0\leq s\leq t_0}\|\varphi(s)-\phi(s)\|^2 + M_1 \\ &\quad + \frac{1}{2(\theta+1)}l\overline{q}\|C\|\sup_{\overline{q}t_0\leq s\leq t_0}\|\varphi(s)-\phi(s)\|^2\sum_{j=1}^{n}q_j(1+q_j^{-1}t_0)^{\theta+1} \\ &\leq \frac{1}{2}M\sup_{\overline{q}t_0\leq s\leq t_0}\|\varphi(s)-\phi(s)\|^2,\end{aligned} \tag{12}$$

where

$$M = [(1+t_0)^{\theta} + 2M_1(\sup_{\overline{q}t_0<s\leq t_0}\|\varphi(s)-\phi(s)\|^2)^{-1} + \frac{1}{\theta+1}l\overline{q}\|C\|\sum_{j=1}^{n}q_j(1+q_j^{-1}t_0)^{\theta+1}] \geq 1,$$

$$M_1 = \frac{1}{2\varepsilon}(k(t_0) - k^*)^2.$$

From (11) and (12), we obtain

$$\frac{1}{2}(1+t)^\theta e(t)^T e(t) \le V(t) \le V(t_0) \le \frac{1}{2}M \sup_{\overline{q}t_0 \le s \le t_0} \|\varphi(s) - \phi(s)\|^2,$$

that is

$$\|e(t)\|^2 \le M \sup_{\overline{q}t_0 \le s \le t_0} \|\varphi(s) - \phi(s)\|^2 (1+t)^{-\theta},\ t \ge t_0,$$

therefore, systems (1) and (2) can achieve GPS under controller (4). □

Remark 1. *Using the definition and properties of the 2-norm, we constructed a Lyapunov functional and derived Theorem 1, which were rarely seen in previous works.*

Remark 2. *This paper introduces polynomial functions* $(1+t)^\theta$ *and* $(1+q_j^{-1}s)^\theta$*, designs controller (4) and constructs Lyapunov functional, which play a crucial role in the proof of GPS.*

In controller (4), if $\theta = 0$, the GPS of systems (1) and (2) degenerates to GAS.

Corollary 1. *If Assumption 1 holds, and the controller is as follows:*

$$\Theta(t) = -k(t)e(t), \tag{13}$$

where $k(t)$ *represents the gain coefficient function,* $\dot{k}(t) = \varepsilon e(t)^T e(t), k(0) \ge 0, \varepsilon > 0$*. Then systems (1) and (2) can achieve GAS under controller (13).*

Remark 3. *Earlier works [3,43] are limited to constant delay systems and cannot accurately capture time-varying delay properties. In [44], although the time-varying delay model extends the constraints of constant delay, bounded derivative is still needed to ensure stability. The system studied in this article is an unbounded proportional delay system, and its analysis does not restrict delay change rate.*

Remark 4. *The GAS of Cohen-Grossberg PDNNs by designing an adaptive controller was investigated in [45]. In this paper, polynomial-type functions are introduced to construct a novel adaptive controller and a Lyapunov functional, a criterion for GPS is established for PDNNs. Compared with GAS, GPS provides explicit information on the convergence order and exhibits a faster convergence rate, thereby offering a more accurate characterization of the dynamic behavior of the system states. In this process, the introduction of the polynomial function plays a critical role in ensuring the GPS of the system.*

Remark 5. *In systems (1) and (2), if* $q_j = 1, j \in \hat{n}$*, systems (1) and (2) become time-delay-free systems, and the conclusions of this paper still hold.*

4. A Numerical Example and Application

4.1. A Numerical Example and Simulations

Example 1. *Take the subsequent PDNNs as the drive system:*

$$\dot{u}(t) = -Au(t) + Bf(u(t)) + Cg(u(qt)), \tag{14}$$

select the parameters of the system as:

$$A = \mathrm{diag}(1.5, 1.2), \quad B = \begin{pmatrix} -1.2 & 1.3 \\ -7.7 & 4.1 \end{pmatrix}, \quad C = \begin{pmatrix} 3.2 & -2.9 \\ 7.1 & -23 \end{pmatrix}, \quad q_1 = q_2 = 0.8,$$

$$f(u(t)) = (\tanh(u_1(t)), \tanh(u_2(t)))^T,\ g(u(qt)) = (\tanh(u_1(q_1 t)), \tanh(u_2(q_2 t)))^T,$$

at this point, $f_j(\cdot)$ *and* $g_j(\cdot)$ *conform to Assumption 1, and* $L_j = M_j = 1, j = 1, 2$*. Under the initial value* $u(0) = (0.1, 0.1)^T$*, the phase diagram (PD) of system (14) is displayed in Figure 1.*

The response system corresponding to system (14) is:

$$\dot{V}(t) = -Av(t) + Bf(v(t)) + Cg(v(qt)) + \Theta(t) \tag{15}$$

with $v(0) = (-0.7, 1.5)^T$*, the PD of system (15) without the controller is shown in Figure 2a. From Figures 1 and 2a, it can be observed that although the their PDs are both chaotic, they are completely different.*

After adding controller (4), when $\varepsilon = 0.9, \theta = 1.3$, the PD of system (15) in Figure 2b is consistent with the PD of system (14) in Figure 1 except for the initial part. This indicates that controller (4) we designed is effective.

In addition, there is a significant difference in the state trajectorys (STs) of systems (14) and (15) without the controller, as shown in Figure 3a,b; Comparing Figure 3a,c, except for the initial part, under the controller (4), the STs of systems (14) and (15) tend to be consistent. In controller (13), still taking $\varepsilon = 0.9$, systems (15) and (14) tend to be consistent except for the initial part, as shown in Figure 4.

For the intial value $e(0) = (-0.8, 1.4)^T$ of the error system, Figure 5a depicts the GPS of systems (14) and (15) under controller (4), and (b) depicts the GAS of systems (14) and (15) under controller (13). As shown in Figure 5a,b, GPS under controller (4) achieves synchronization at t = 5.41, and GAS under controller (13) at t = 6.77. Thus, GPS has a faster convergence rate than GAS. The difference between controller (4) and controller (13) is the introduction of a polynomial function, which verifies the crucial role of introducing the polynomial function in improving the synchronization efficiency.

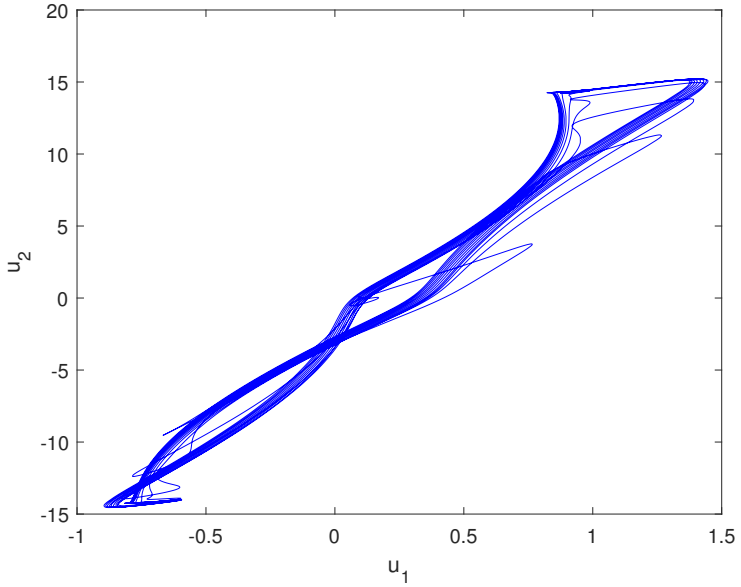

Figure 1. PD of system (14).

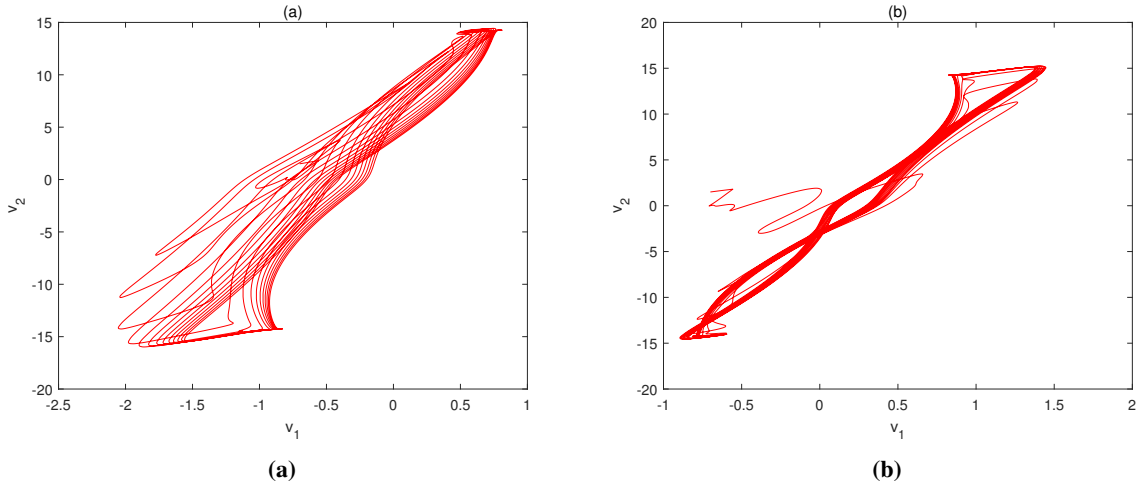

(a) **(b)**

Figure 2. PDs of system (15): (**a**) without a controller; (**b**) with controller (4).

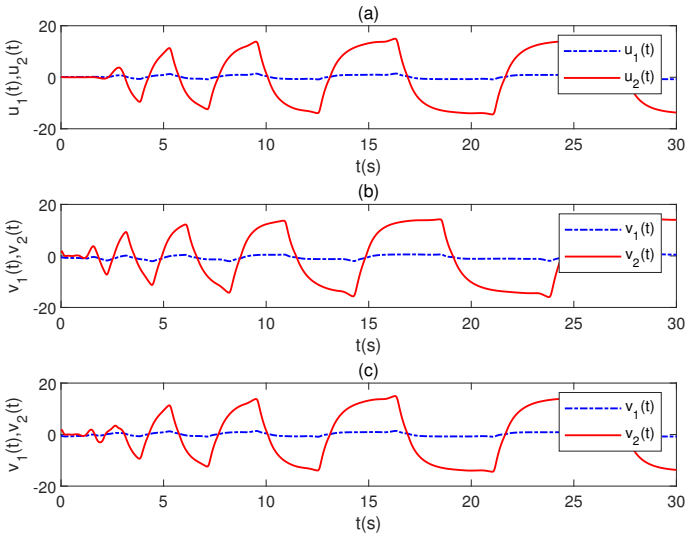

(a)

Figure 3. (**a**) ST of system (14); (**b**) ST of system (15) without the controller; (**c**) ST of system (15) with controller (4).

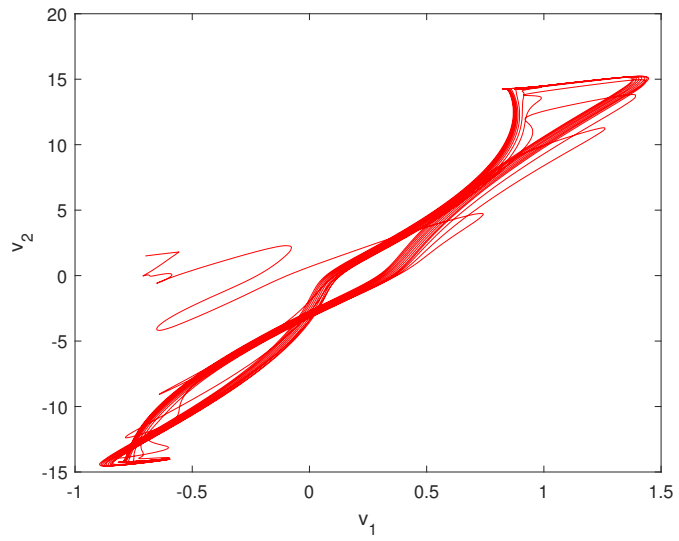

(a)

Figure 4. PD of system (15) with controller (13).

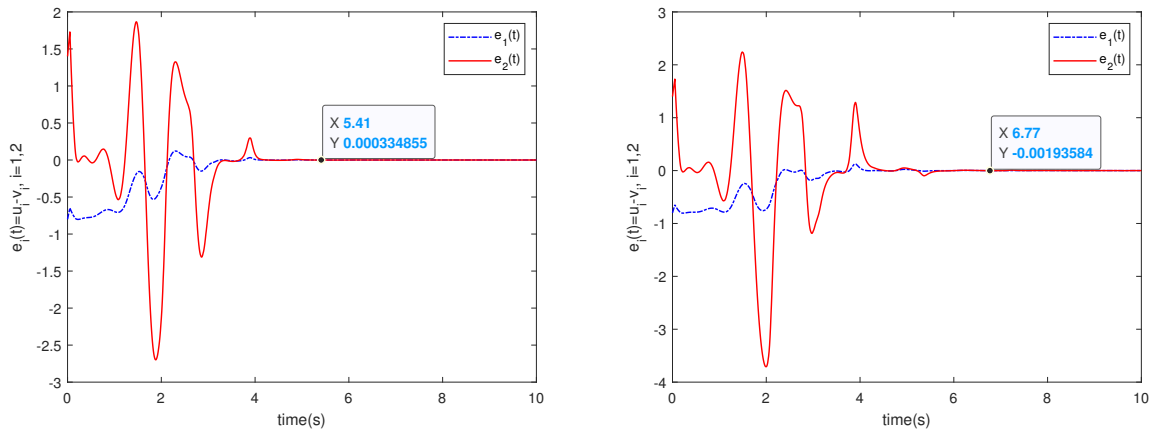

(a) **(b)**

Figure 5. (**a**) STs of the error system of systems (14) and (15): under controller (4); (**b**) under controller (13).

In contrast, if $q_1 = q_2 = 1$ in systems (14) and (15), other conditions have not changed, their PDs are shown in Figure 6. It can be observed that the PDs in Fig. 6 are periodic, while Figures 1 and 2a with proportional delays are chaotic. They are completely different, and the proportional delays cause this situation to occur. From Remark 5, systems (14) and (15) are synchronized under controllers (4) and (13), as shown in Figure 7.

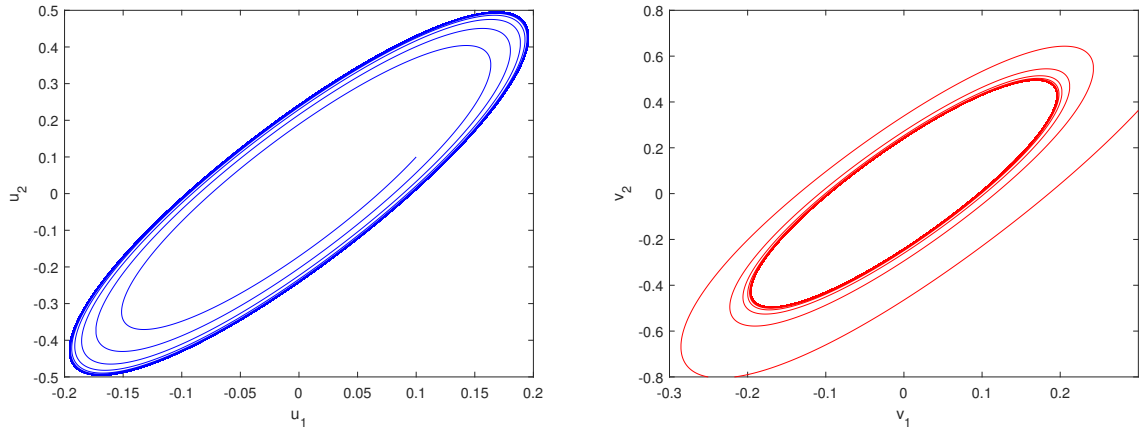

(a) **(b)**

Figure 6. Systems without delay: (**a**) PD of (14); (**b**) PD of (15) without the controller.

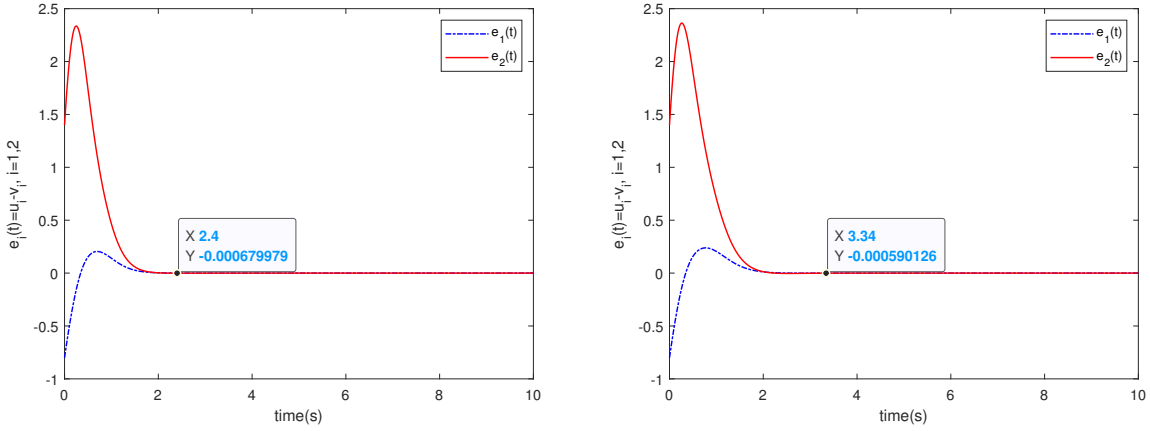

(a) **(b)**

Figure 7. (**a**) STs of the error system of systems without delay (14) and (15): under controller (4); (**b**) under controller (13).

4.2. Application of GPS in Image Encryption

Next, this section will explore the practical applications of adaptive synchronization control. The adaptive GPS in this paper is applied to the field of image encryption here. Based on PDNNs (14) and (15) construct in Example 1 under controller (4), this paper applies their adaptive synchronization characteristics to the design of an image encryption algorithm. In terms of security verification, through the analysis of histogram distribution, information entropy, synchronization error curves, and scatter plots, the security performance of this encryption scheme is verified.

As presented in Figure 8a, select the image A of size $M \times N \times 3$ and use systems (14) and (15) synchronized under controller (4) to encrypt and decrypt the image A. The process is as follows:

(i) Pixel reading. The pixel values in A range from 0 to 255 and are retrieved from R, G, B channels. Read the color image A to be encrypted, and save the original pixel values in matrix form as R_a, G_a, and B_a for the three channels of R (red), G (green), and B (blue) respectively.

(ii) Permutation encryption. Generating two groups of pseudo-random sequences D_1 and D_2 of length $M \times N$. Through D_1, perform permutation encryption on matrices R_a, G_a, and B_a respectively. Merge the three-channel matrixs to obtain the permutation-encrypted image.

(iii) Image Encryption. Encrypt the image based on the model parameters and initial values given in Example 1. Sequence of system (14) can be obtained and intercepted. This sequence can be obtained through D_1, and (u_1, u_2) is generated in the following way. An $M \times N$ data sequence is selected, with Loc serving as the sequence capture variable to capture it. The detailed conversion process is presented below (using sequence for illustration):

$$Loc = 10000; u_1(i) = u_1 + Loc : (M \times N) + Loc,$$

the matrix-form key corresponding to the original image formed by $(u_1, u_2)^T$:

$$\begin{aligned} r &= \mathrm{mod}\big(\mathrm{round}\big((|u_1 + u_2|) \times 10^8\big), 257\big), \\ g &= \mathrm{mod}\big(\mathrm{round}\big((|3u_1 - u_2|) \times 10^8\big), 256\big), \\ b &= \mathrm{mod}\big(\mathrm{round}\big((|u_1 + 2u_2|) \times 10^8\big), 256\big). \end{aligned}$$

Merge the matrices r, g, b to obtain the key. Perform an XOR operation on the image A and the key to get the encrypted image A', as demonstrated in Figure 8b.

(iv) Image decryption. Based on Example 1, for the sequence obtained from the response system, perform a permutation through D_1 to obtain sequence $(v_1, v_2)^T$. Generate the decryption key according to the same rules as the encryption process, perform an XOR operation on image A', and then perform a permutation restoration to obtain image A'' (see Figure 8c) to complete the decryption.

The findings of the experiment are presented in Figure 8a–c. More specifically, the encrypted image A' generated from the sequence of system (14) is illustrated in Figure 8b. It significantly conceals the information inherent in the original image A. In addition, Figure 8c demonstrates the decrypted image A'' reconstructed utilizing the sequence from system (15), which indicates that the encrypted image A' has been completely restored to its original state A. Subsequently, a more detailed analysis was conducted on the security of the proposed image encryption algorithm.

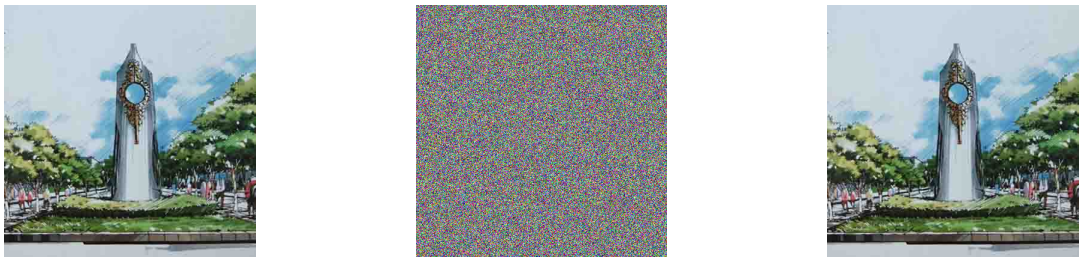

(a) **(b)** **(c)**

Figure 8. (**a**) Original image; (**b**) Image encrypted by system (14); (**c**) Image decrypted by system (15).

A histogram is used to verify whether an encryption algorithm can hide the statistical characteristics of the original image, and its degree of equalization is an important criterion for evaluating the performance of the encryption algorithm. An ideal encryption system should make the histogram distribution of the encrypted image approach a uniform state. In this state, it indicates that the statistical pattern of the original data has been completely destroyed, and there is no effective information left in the ciphertext that can be used for decryption. As depicted in Figure 9a–f, this paper conducts a in-depth analysis of the histograms of R, G, B. The data in Figure 9a–c has obvious peak regions, reflecting the "information bias" of the original data. Figure 9d–f illustrates that the histograms of the encrypted images exhibit highly consistent and uniform distribution characteristics. The distribution change "from non-uniform to uniform" reflects the scrambling effect of the encryption algorithm on the original data. It effectively conceals the information characteristics of the original data, resists potential statistical analysis attacks, and prevents attackers from inferring the original image information through probability distribution, thereby significantly improving security. This proves the effectiveness and accuracy of the image encryption method proposed in this paper.

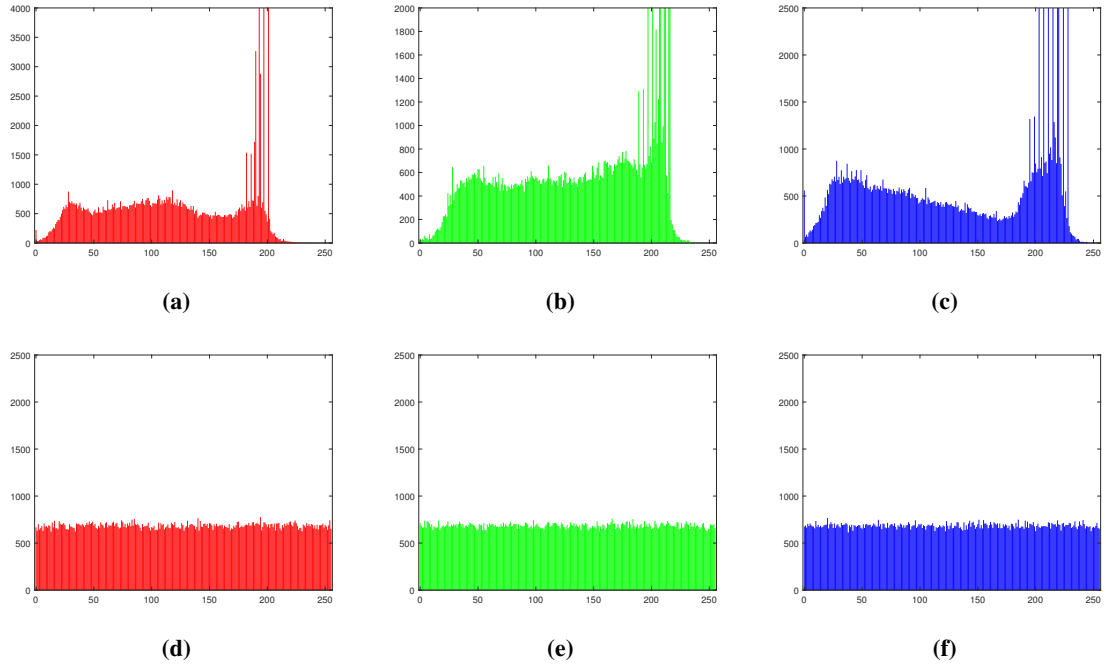

Figure 9. (**a**)–(**c**): R, G, B Histogram of A; (**d**)–(**f**): R, G, B Histogram of A'.

The information entropy of an image measures the uncertainty or randomness of pixel values in the image. The definition of information entropy is

$$Q(\sigma) = -\sum_{i=0}^{n} p(\sigma_i) \log_2 p(\sigma_i),$$

where $p(\sigma_i)$ denotes the probability of the pixel gray value s_i occurring. The greater the information entropy value $Q(\sigma)$, the higher the degree of chaos in the image or the more uniform the distribution of pixel grayscale values, that is, the more uniform the data distribution and the stronger the randomness of the information. When the information entropy of the encrypted image approaches the theoretical maximum value of 8, it indicates that the encryption operation has successfully broken the concentrated distribution of the original image, effectively eliminated the statistical characteristics of the original data, significantly improved the randomness of the information, enhanced security, and met the cryptographic security standards. Figure 8a–c is demonstrated in Table 2. With the information entropy of the encrypted image reaching 7.9914, it can be inferred that the encrypted image has distinct chaotic characteristics and enhanced security. The information entropy of the original image and the decrypted image is basically the same, both approximately 6.5468. This indicates that the encryption algorithm achieves information hiding, and the decryption operation can effectively restore the distribution characteristics of the original information.

To effectively defend against statistical attacks between adjacent pixels, it is crucial to reduce the information correlation between pixels. Table 3 quantitatively analyzes the correlation characteristics of adjacent pixels in the horizontal, vertical, and diagonal dimensions of the image. The experimental data illustrate that the correlation coefficients of adjacent pixels in the R, G, B-image components encrypted in the horizontal, vertical, and diagonal directions are all close to zero. These data fully verify that the encryption algorithm can efficiently eliminate the correlation between pixels, thereby significantly improving the robustness of the system against statistical attacks.

Figure 10a–f visually displays the changes in pixel correlation before and after encryption. The scatter plots of the original image in the horizontal, vertical, and diagonal directions, as depicted in Figure 10a–c, present an obvious linear distribution, denoting that a strong association—the numerical variation patterns of adjacent pixels are highly consistent exist between adjacent pixels. In comparison, the scatter plots of the encrypted image, as presented in Figure 10d–f, exhibit a uniform distribution. The pixels in the three directions have no obvious correlation, and show weak correlation, which means strong randomness. Attackers find it difficult to infer the image content through the correlation of adjacent pixels, which verifies that the encryption algorithm can effectively destroy the statistical relationship between pixels and ensure the privacy and security of the image. Figures 8–10 as well as Tables 2 and 3 are implemented by MATLAB programming.

Table 2. Image information entropy.

Figure 8a	Figure 8b	Figure 8c
6.5468	7.9914	6.5468

Table 3. Correlations between two adjacent pixels of color images.

Direction	Image	R	G	B
Horizontal	Original	0.9980	0.9987	0.9992
	Encrypted	−0.0039	−0.0083	−0.0118
	Decrypted	0.9980	0.9987	0.9992
Vertical	Original	0.9992	0.9994	0.9996
	Encrypted	0.0220	0.0015	−0.0031
	Decrypted	0.9992	0.9994	0.9996
Diagonal	Original	0.9961	0.9973	0.9983
	Encrypted	−0.0322	0.0002	0.0200
	Decrypted	0.9961	0.9973	0.9983

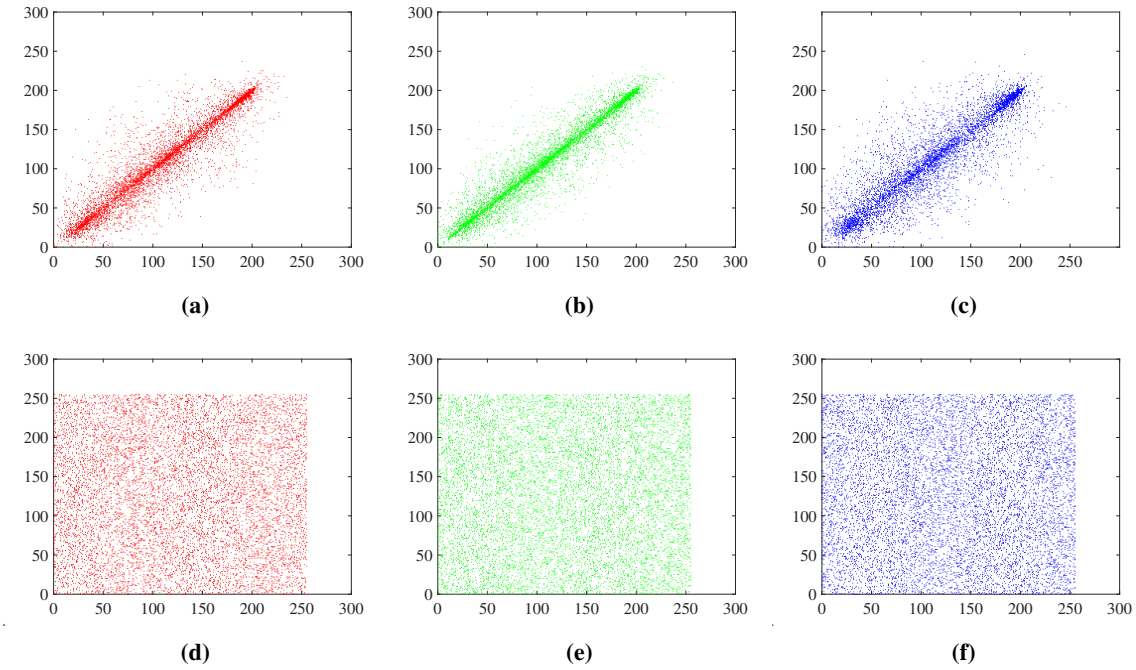

Figure 10. Scatter plots: (**a**)–(**c**) adjacent horizontal, vertical and diagonal pixels in A; (**d**)–(**f**) adjacent horizontal, vertical and diagonal pixels in A'.

The above experimental verification of the encryption algorithm, together with the earlier validation of PDNNs adaptive synchronization, provides comprehensive support for the conclusions of this study.

5. Conclusions

This paper investigates the adaptive synchronization problem of PDNNs. By introducing polynomial functions, designing adaptive controllers, and constructing appropriate Lyapunov functional. Through a numerical example and simulations, the accuracy of the obtained criteria is further verified. Meanwhile, this paper applies the adaptive GPS of the drive-response systems to image encryption and decryption, and uses MATLAB to conduct experimental analyses on histograms, information entropy, synchronization errors, and scatter plots. The results illustrate that the synchronization scheme and encryption algorithm designed in this paper perform excellently in image encryption and decryption, successfully realizing the important application of synchronization control of PDNNs in the field of

image encryption. The limitations of this paper lie in focusing only on adaptive synchronization, not considering event-triggered synchronization and adaptive pinning synchronization, nor the impact of uncertain parameters, and the delay model is relatively simple. In the future, we will consider researching memristive NNs, adopt adaptive pinning synchronization, and apply the synchronization results to secure communication.

Author Contributions

Q.Y.: writing—original draft; X.H.: writing—review and editing; L.Z.: investigation ; M.Z.: investigation. All authors have read and agreed to the published version of the manuscript.

Funding

This work is supported Natural Science Foundation of Tianjin, China (No. 24JCYBJC00470).

Institutional Review Board Statement

Not applicable.

Informed Consent Statement

Not applicable.

Data Availability Statement

All research data produced in this study are contained in this article.

Conflicts of Interest

The authors declare no conflict of interest. Given the role as Editorial Board Members, Liqun Zhou had no involvement in the peer review of this paper and had no access to information regarding its peer-review process. Full responsibility for the editorial process of this paper was delegated to another editor of the journal.

Use of AI and AI-Assisted Technologies

During the preparation of this work, the authors used deepseek to simplify Table 1 and polish the descriptive part related to image encryption. After using this tool/service, the authors reviewed and edited the content as needed and take full responsibility for the content of the published article.

References

1. Hopfield, J. Neurons with graded response have collective computational properties like those of two state neurons. *Proc. Natl. Acad. Sci. USA* **1984**, *81*, 3088–3092.
2. Pecora, L.; Carroll, T. Synchronization in chaotic system. *Phys. Rev. Lett.* **1990**, *64*, 821–824.
3. Lu, J.; Cao, J. Adaptive synchronization of uncertain dynamical networks with delayed coupling. *Nonlinear Dyn.* **2008**, *53*, 107–115.
4. Wang, L.; Shen, Y.; Yin, Q.; et al. Adaptive synchronization of memristor-based neural networks with time-varying delays. *IEEE Trans. Neural Netw. Learn. Syst.* **2015**, *26*, 2033–2042.
5. Zhang, K.; Li, J.; Song, H. Collocation methods for nonlinear convolution Volterra integral equations with multiple proportional delays. *Appl. Math. Comput.* **2012**, *218*, 10848–10860.
6. Zhou, L. On the global dissipativity of a class of cellular neural networks with multi-pantograph delays. *Adv. Artif. Neural Syst.* **2011**, *2011*, 941426.
7. Zhou, L. Global asymptotic stability of cellular neural networks with proportional delays. *Nonlinear Dyn.* **2014**, *77*, 41–47.
8. Zhang, C.K.; He, Y.; Jiang, L.; et al. Delay-dependent stability criteria for generalized neural networks with two delay components. *IEEE Trans. Neural Netw. Learn. Syst.* **2013**, *25*, 1263–1276.
9. Wang, X.; Park, J.; Yang, H.; et al. Delay-dependent stability analysis for switched stochastic networks with proportional delay. *IEEE Trans. Cybern.* **2020**, *52*, 6369–6378.
10. Gao, X.; Li, Y.; Liu, X.; et al. Stability analysis of fractional bidirectional associative memory neural networks with multiple proportional delays and distributed delays. *IEEE Trans. Neural Netw. Learn. Syst.* **2025**, *36*, 738–752.
11. Wang, L.; Ge, M.F.; Hu, J.; et al. Global stability and stabilization for inertial memristive neural networks with unbounded distributed delays. *Nonlinear Dyn.* **2019**, *95*, 943–955.
12. Zhou, L.; Zhao, Z.; Zhu, Q.; et al. Global polynomial stabilization of impulsive neural networks with bidirectional proportional delays. *IEEE Trans. Netw. Sci. Eng.* **2023**, *11*, 471–484.

13. Kong, F.; Zhu, Q. Fixed-time stabilization of discontinuous neutral neural networks with proportional delays via new fixed-time stability lemmas. *IEEE Trans. Neural Netw. Learn. Syst.* **2021**, *34*, 775–785.
14. Zhou, R.; Zhou, L. Global polynomial stabilization and global asymptotic stabilization of coupled neural networks with multi-proportional delays. *Math. Meth. Appl. Sci.* **2020**, *43*, 7345–7360.
15. Guan, K.; Yang, J. Global asymptotic stabilization of cellular neural networks with proportional delay via impulsive control. *Neural Process. Lett.* **2019**, *50*, 1969–1992.
16. Long, C.; Zhang, G.; Zeng, Z.; et al. Finite-time stabilization of complex-valued neural networks with proportional delays and inertial terms: A non-separation approach. *Neural Netw.* **2022**, *148*, 86–95.
17. Liu, J.; Xu, R. Passivity analysis and state estimation for a class of memristor-based neural networks with multiple proportional delays. *Adv. Differ. Equ.* **2017**, *2017*, 34.
18. Zhang, H.; Wang, C.; Ye, R.; et al. Novel order-dependent passivity conditions of fractional generalized Cohen-Grossberg neural networks with proportional delays. *Commun. Nonlinear Sci. Numer. Simul.* **2023**, *128*, 107155.
19. Zhang, J.; Zhu, S. Passivity and robust passivity of impulsive inertial neural networks with proportional delays under the non-reduced order approach. *Neurocomputing* **2024**, *575*, 127322.
20. Han, J. Finite-time passivity and synchronization for a class of fuzzy inertial complex-valued neural networks with time-varying delays. *Axioms* **2024**, *13*, 39.
21. Zhou, L. Dissipativity of a class of cellular neural networks with proportional delays. *Nonlinear Dyn.* **2023**, *73*, 1895–1903.
22. Xing, L.; Zhou, L. Polynomial dissipativity of proportional delayed BAM neural networks. *Int. J. Biomath.* **2020**, *13*, 2050050.
23. Aouiti, C.; Sakthivel, R.; Touati, F. Global dissipativity of fuzzy cellular neural networks with inertial term and proportional delays. *Int. J. Syst. Sci.* **2020**, *51*, 1392–1405.
24. Li, N.; Cao, J. Global dissipativity analysis of quaternion-valued memristor-based neural networks with proportional delay. *Neurocomputing* **2018**, *321*, 103–113.
25. Son, D.T.; Trinh, H. On global dissipativity of nonautonomous neural networks with multiple proportional delays. *IEEE Trans. Neural Netw. Learn. Syst.* **2016**, *29*, 225–231.
26. Huang, C.; Zhang, H. Periodicity of non-autonomous inertial neural networks involving proportional delays and non-reduced order method. *Int. J. Biomath.* **2019**, *12*, 1950016.
27. Xu, C. Global exponential periodicity for fuzzy cellular neural networks with proportional delays. *J. Intell. Fuzzy Syst.* **2017**, *33*, 829–839.
28. Yang, H. Weighted pseudo almost periodicity on neutral type CNNs involving multi-proportional delays and D operator. *AIMS Math.* **2021**, *6*, 1865–1879.
29. Kong, F.; Ren, Y.; Sakthivel, R. New criteria on periodicity and stabilization of discontinuous uncertain inertial Cohen-Grossberg neural networks with proportional delays. *Chaos Solitons Fractals* **2021**, *150*, 111148.
30. Zhou, L.; Zhang, Y. Global exponential periodicity and stability of recurrent neural networks with multi-proportional delays. *ISA Trans.* **2016**, *60*, 89–95.
31. Zhou, L.; Zhao, Z. Exponential synchronization and polynomial synchronization of recurrent neural networks with and without proportional delays. *Neurocomputing* **2020**, *372*, 109–116.
32. Zhou, L.; Zhu, Q.; Huang, T. Global polynomial synchronization of proportional delayed inertial neural networks. *IEEE Trans. Syst. Man Cybern. Syst.* **2023**, *53*, 4487–4497.
33. Yan, W.; Zhou, L. Fixed-time synchronization of discontinuous proportional delay inertial neural networks with uncertain parameters. *Inf. Sci.* **2024**, *678*, 120931.
34. Zhang,J.; Li, Z.; Cao, J.; et al. Global Polynomial Synchronization of Quaternion-Valued Inertial Neural Networks With Proportional Delay and Mismatched Parameters. *Math. Meth. Appl. Sci.* **2025**, *48*, 11113–11123.
35. Zhang, Y.; Zhou, L. State estimation for proportional delayed complex-valued memristive neural networks. *Inf. Sci.* **2024**, *680*, 121150.
36. Zhang, Y.; Zhou, L. Stabilization and lag synchronization of proportional delayed impulsive complex-valued inertial neural networks. *Neurocomputing* **2022**, *507*, 428–440.
37. Han, J.; Zhou, L. Finite-time synchronization of proportional delay memristive competitive neural networks. *Neurocomputing* **2024**, *610*, 128612.
38. Li, Q.; Zhou, L. Global asymptotic synchronization of inertial memristive Cohen–Grossberg neural networks with proportional delays. *Commun. Nonlinear Sci. Numer. Simul.* **2023**, *123*, 107295.
39. Wan, Y.; Zhou, L.; Han, J. Global polynomial synchronization of proportional delay memristive neural networks with uncertain parameters and its application to image encryption. *Eng. Appl. Artif. Intell.* **2025**, *147*, 110290.
40. Han, J.; Zhou, L. Fixed-time synchronization of proportional delay memristive complex-valued competitive neural networks. *Neural Netw.* **2025**, *188*, 107411.
41. Wang, Y.; Zhou, L. General decay projection synchronization of proportional delay memristive competitive neural networks with uncertain parameters for image encryption. *Inf. Sci.* **2025**, *712*, 122136.
42. Zhou, L.; Hang, J.; Zhao, Z.; et al. Global polynomial synchronization of proportional delay memristive competitive neural

networks with uncertain parameters for image encryption. *IEEE Trans. Syst. Man Cybern. Syst.* **2025**, *55*, 5424–6434.

43. Bao, H.; Park.; Cao, J. Adaptive synchronization of fractional-order memristor-based neural networks with time delay. *Nonlinear Dyn.* **2015**, *82*, 1343–1354.
44. Zhang, X.; Han, Q.; Seuret, A.; et al. Overview of recent advances in stability of linear systems with time-varying delays. *IET Control Theory Appl.* **2019**, *13*, 1–16.
45. Jia, S.; Hu, C.; Yu, J.; Jiang, H. Asymptotical and adaptive synchroniza tion of cohen-grossberg neural networks with heterogeneous proportional delays. *Neurocomputing* **2018**, 275, 1449–1455.
46. Zhang, H; Zhou, Y; Zeng, Z. Master-slave synchronization of neural networks with unbounded delays via adaptive method. *IEEE Trans. Cybern.* **2023**, *53*, 3277–3287.